A Non-equilibrium STM model for Kondo Resonance on surface

Wei Fan
Key Laboratory of Materials Physics, Institute of Solid State Physics,
Chinese Academy of Sciences, 230031-Hefei, People's Republic of China

Based on a no-equilibrium STM model, we study Kondo resonance on a surface by self-consistent calculations. The shapes of tunneling spectra are dependent on the energy range of tunneling electrons. Our results show that both energy-cutoff and energy-window of tunneling electrons have significant influence on the shapes of tunneling spectra. If no energy-cutoff is used, the Kondo resonances in tunneling spectrum are peaks with the same shapes in the density of state of absorbed magnetic atoms. This is just the prediction of Tersoff theory. If we use an energy cutoff to remove high-energy electrons, a dip structure will modulate the Kondo resonance peak in the tunneling spectrum. The real shape of Kondo peak is the mixing of the peak and dip, the so-called Fano line shape. The method of self-consistent non-equilibrium matrix Green function is discussed in details.

PACS numbers: 68.37.Ef, 73.23.-b, 72.10.-d, 73.20.-r

I. INTRODUCTION

Scanning Tunneling Microscope (STM) has been widely used to study atomic and electronic structures of surface and atoms absorbed on it. A currently interesting topic is Kondo effect of magnetic atoms on non-magnetic metal surface. The interest along this direction is motivated by recent advance in the construction of novel nano-structure device on surface. STM has been used to probe the Kondo resonance of a single magnetic atom.[1, 2, 3, 4, 5, 6] The magnetic cobalt phthalocyanine molecule absorbed on Au(111) surface shows Kondo effect by having cut away eight hydrogen from the molecule. [7] Kondo resonance haven been found in other magnetic molecules absorbed on metal surfaces such as $Co(CO)_n$ molecules on Cu(100) surface [8]. Additionally, STM has also been used to study the formation of Kondo molecule.[9, 10] The most interesting phenomenon is so called Quantum Mirage [11, 12] due to the refocus of Kondo resonance on surface.

Generally STM tunneling spectrum isn't exactly correspondent to the atomic and electronic structure of the surface. To obtain the realistic atomic and electronic structure from STM tunneling spectrum, it is valuable to establish a believable STM theoretical model that is related the realistic atomic structure or electronic structure to the STM tunneling spectrum. Based on the Tersoff alike theory,[13, 14, 15, 16] the differential conductance of electronic tunneling in STM is proportional to the Local Density of State (LDOS) of surface state. The resonance peak at zero-bias voltage in dI/dV curve is generally the mixing of Kondo resonance with other resonance such as d-resonance from 3d magnetic atom.[2] The STM models based on Anderson Model have successfully explained the Fano shape of Kondo resonance using the equilibrium many-body theory [17, 18, 19, 20, 21] and non-equilibrium theory.[22]

Electronic address: fan@theory.issp.ac.cn

Quantum tunneling of electrons in STM device is out of equilibrium in nature. In this paper, using a non-equilibrium self-consistent method, we calculate the STM tunneling spectra for magnetic atoms on metal surface. Kondo effect can be solved using analytical or numerical methods, such as, the Non-Crossing Approximations (NCA) and other Larger N methods are suited for the infinite U Anderson model.[23, 24, 25] The numerical renormalization group (NRG) and the exact Bethe Ansatz need to linearize the dispersion relation near Fermi energy after having simplified into one-dimension model.[23] The method used in this paper is similar to the iterative perturbation theory (IPT).[26, 27] The big difference is that in this work the Kondo resonance peak is decoupled from other parts of the Green function. However for IPT, the Kondo resonance is imported into the Green function of magnetic atom by interpolating $\frac{2}{0}$ self-energy into an appropriate self-energy ansatz. The decoupled scheme in this work can be obtained by more detail theoretical analysis such as in reference.[28]

As a company of Kondo resonance, the so-called zero-bias anomaly has contribution to the differential conductance near zero-bias voltage. The zero-bias voltage anomaly may have different origins such as the orthogonality catastrophe [29] and the co-tunneling mechanism [30, 31]. The electrons have no enough energies for most of many-body events at small bias voltage. The zero-bias anomaly appears as a local minimum in dI/dV curves near zero-bias voltage.

Experimentally Kondo resonance in dI/dV curves are clear dip structures for single absorbed magnetic atoms [1, 2, 3, 4] but peak structures for absorbed magnetic molecules [7, 8]. In this paper, the signals of Kondo resonance from the dI/dV curves are Fano-line shapes and are the mixing of Kondo resonance and dip structure due to zero-bias anomaly. This is well consistent with experimental observations. The zero-bias anomaly generally appears as a dip structure near zero-bias and is frequently covered by background noise. If other resonance peak appears at zero bias, the zero-bias anomaly can shows itself by modulating the resonance

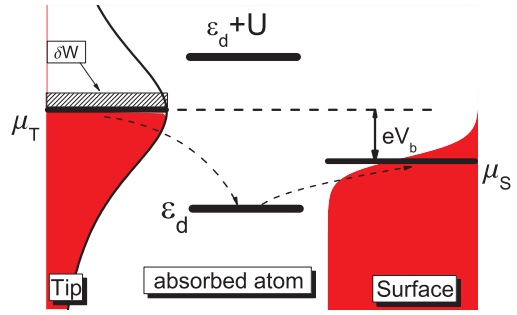

FIG. 1: The energy-level distribution of the STM device. Two horizontal lines labelled with $_T$ and $_S$ illustrate the chemical potentials of the tip and the surface. The $_S$ is the chemical potential for the surface where the Kondo resonance happens. The red areas show the states of the tip and surface, which are filled with electrons. The chemical potential $_S$ of the surface is fixed to zero. The difference of the chemical potentials for the tip and the surface is induced by the bias voltage V_b applied to the surface. Two thick bold lines present the splitting energy-levels for magnetic atom due to the on-site coulomb interaction. Two curved dash lines show a cotunneling event in the STM device.

peak. This is why Kondo resonance generally appears company with a local minimum in dI/dV curves. If we properly reduce the back ground noise, the dip structure also can be observed in the tunneling spectra. The shapes of tunneling spectra are dependent on the energy-range of tuneling electrons. The paper is organized as following, after brief introduction we present the theoretical STM model in section two. In the section three, we present the non-equilibrium self-consistent method in detail. Our main results are presented in section four. Two appendixes are at the end of the paper which include the brief introduction of the matrix representation of non-equilibrium Green function and the derivation of the tunneling-current formulations.

II. THEORETICAL STM MODEL

The Non-equilibrium Green-function method (Schwinger-Keldysh Contour) [32, 33, 34, 35, 36] has been used successfully to study the mesoscopic quantum transport of quantum dots and others mesoscopic quantum device.[37, 38, 39, 40, 41, 42] The model Hamiltonian is splitting two parts $H = H_0 + H_T$. H_T is the tunneling Hamiltonian which expresses the electronic transport between different parts of the STM device such as tip, surface and absorbed atom shown in [Fig. 1].

$$H_0 = \sum_k \varepsilon_{pk}\, p^y_k p_k + \sum_n \varepsilon_{tn}\, t^y_n t_n + \sum_{} \varepsilon_{} d^y d + U d^y_{"} d_{"} d^y_{\#} d_{\#}; \quad (1)$$

$$H_T = \sum_{n\,\sigma} V_{n\,\sigma} t^y_{n\,\sigma} d_\sigma + \sum_{k\,\sigma} A_{k\,\sigma} p^y_{k\,\sigma} d_\sigma + \sum_{nk\,\sigma} B_{nk\,\sigma} p^y_{k\,\sigma} t_{n\,\sigma} + h.c: \quad (2)$$

$p^y; t^y; d^y$ and $p; t; d$ are the electron creation and annihilation operators of surface, tip and absorbed atom respectively. $V_{n\,\sigma}$, $B_{nk\,\sigma}$ and $A_{k\,\sigma}$ are the tunneling matrix elements or hybridizing matrix elements between the tip and absorbed atom, the tip and surface, and the absorbed atom and surface. k is the energy-level index of the surface, n the STM tip and σ is the spin index of electron. ε_{pk}, ε_{tn} and $\varepsilon_{}$ are the energy levels of the surface, the tip and the absorbed atom respectively. U is the on-site Coulomb energy of the absorbed atom. The hybridization Hamiltonian, the second term of H_T, has the same form as the tunneling Hamiltonian. Thus hybridization can treat the same foot as the tunneling events.

The STM probes the tunneling current or the change of charges in the tip when a bias voltage applies to the surface. The operator of electron number at the tip is written as $N_T = \sum_n t^y_n t_n$ and the electronic current is its time-derivative of $J_T = e\frac{dN_T}{dt} = \frac{ie}{\hbar}[N_T(t); H]$. After having been calculated the commutations the current is expressed as

$$\langle J_T\rangle = \frac{2e}{\hbar} Re\Big(\sum_{n\,\sigma} V_{n\,\sigma}\langle t^y_{n\,\sigma} d_\sigma\rangle^< + \sum_{nk\,\sigma} B_{nk\,\sigma}\langle t^y_{n\,\sigma} p_{k\,\sigma}\rangle^<\Big); \quad (3)$$

where the lesser Green function $G^<(t;t') = i\langle A(t')^y B(t)\rangle$. The similar formula has appeared in Ref.[22] but replaced the real part with imaginary part. Two formulas are the same if having considered without image unit i in the definition of lesser Green function in that paper. In the appendix B, we derive below current formula using the matrix non-equilibrium Green functions.

$$\langle J_T\rangle = J_1 + J_2 \quad (4)$$

$$J_1 = \frac{2e}{h}\int^c d! \, ReTr[G^{ct(r)}(!)\,\Sigma^{ct(<)}(!)]$$

$$J_2 = \frac{2e}{h}\int^c d! \, ReTr[G^{ct(<)}(!)\,\Sigma^{ct(a)}(!)]:$$

where Tr presents the summation for all energy-level and spin indexes $\sum_{nn'\sigma\sigma'}$. The superscript c indicates that Green functions are matrixes defined in the appendix A. The ^{r}, ^{a}, $^<$ and $^>$ indicate the four elements of the matrix Green function Eq. (A1) and the ^{r} and ^{a} are the retard and advance Green function defined in Eq. (A4).

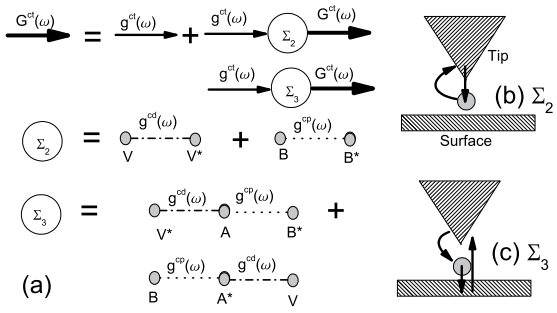

FIG. 2: (a) Feynman diagram representation of Dyson equation for the tip. The Dyson equations for absorbed magnetic atom and surface are similar. (b) The physical event for the first term of the tip self-energy Σ_2 includes two tunneling events. The electron jumps to the absorbed atom and returns to the tip. (c) The physical events for the first term of the tip-energy Σ_3 includes a cotunneling event from the tip to the surface via the absorbed atom and a single tunneling to return to the tip from the surface.

The current J_1 flows into the tip from the surface and absorbed atom, and J_2 flow out of the tip to the surface and absorbed atom. The limitations of integral of the current is dependent on the problem we will consider and can choose Eq. (B7) or Eq. (B8). Near zero bias we need an energy cutoff and Eq. (B8) is a good choice.

III. THE METHODS OF NUMERICAL CALCULATION

The non-equilibrium Green function is defined on a contour with two branches: the positive branch from negative infinite on time axis to positive infinite and the negative branch from positive infinite return to negative infinite. The contour green functions can be replaced by a matrix Greens functions. The matrix Green can be calculated using the standard perturbed methods in the same manner as the zero-temperature Green function in the standard textbook.[34] In Appendix A, we present the main formulas and their computational methods.

A. The key formulas for self-consistent calculation

We assume the Hamilton H_0 can be solved exactly and the tunneling Hamilton treats as perturbations. The self-consistent calculations are used to obtain the full Green functions. At first, we solve the Hamilton H_0 and the obtained Green functions are used as the free Green functions for self-consistent calculations. At the next step, the self-energies are calculated using the Eq. (B5). Three new Green Functions are calculated using three Dyson equations for the tip, adatom and surface, which are expressed as

$$\begin{aligned} G^{ct} &= g^{ct}(!) + g^{ct}(!)\ {}^{ct}(!)G^{ct}(!) \\ G^{cd} &= g^{cd}(!) + g^{cd}(!)\ {}^{cd}(!)G^{cd}(!) \\ G^{cp} &= g^{cp}(!) + g^{cp}(!)\ {}^{cp}(!)G^{cp}(!); \end{aligned} \tag{5}$$

or diagrammatically illustrated in Fig.2. We replace the free Green functions in the self-energy formulas Eq. (B5) with new Green functions.

$$\begin{aligned} {}^{cd}(!) &= \sum_{n'n''} V_{n'0'} V_{n''0''} G^{ct}_{n'n''0'0''}(!) \\ &+ \sum_{k'k''} A_{k'0'} A_{k''0''} G^{cp}_{k'k''0'0''}(!) + {}^{cd}_{3}(!) \\ {}^{cp}_{kl}(!) &= \sum_{n'n''} B_{n'0'k} B_{n''0''l} G^{ct}_{n'n''0'0''}(!) \\ &+ \sum_{0'0''} A_{k\ 0'} A_{l\ 0''} G^{cd}_{0'0''}(!) + {}^{cp}_{3kl}(!) \\ {}^{ct}_{mn}(!) &= \sum_{0'0''} V_{m\ 0'} V_{n\ 0''} G^{cd}_{0'0''}(!) \\ &+ \sum_{k'l'} B_{mk'0'} B_{nl'0''} G^{cp}_{k'l'0'0''}(!) + {}^{ct}_{3mn}(!): \end{aligned} \tag{6}$$

The Eq. (6) and three Dyson equations Eq. (5) form a self-consistent loop. In Fig.2 and Eq. (B6), the $_3$ self-energies represent the cotunneling mechanism which will contribute part of the zero-bias anomaly in dI/dV curve.

B. The free Green functions for the surface and tip

At first, we calculate the equilibrium retarded and advanced Green functions as the free Green functions used in following non-equilibrium self-consistent calculations. The surface is treated as two-dimensional electronic gas. The density of state (DOS) of two-dimensional electronic gas is flat and featherless with 4.0 eV width centered at Fermion energy of the surface. The well-shaped sharp STM tip is constructed with smaller number of atoms. The tip can be modeled as an atomic cluster with discrete energy-levels. Because the electron number is limited, there exists a highest-occupied energy-level such as the HOMO (Highest Occupied Molecular Orbit) energy E_{HOMO} for molecular systems or Fermi-energy for metal, all states with energies less than the highest-occupied energy-level are occupied, and all states with energies larger than the energy-level are empty. The electrons with energies near the energy-level are important to the physical and chemical properties of atomic clusters. Because the tip is in the metal environment, we assume the tip is in metal state and has a sharp Fermi surface. The tip models as a single energy level identified as Fermi energy $_T$. The free retarded Green function for the tip is

written as $g_n^{rt} = \frac{1}{! \ "_{tn} + i_t}$, where $"_{tn} = _T$. The DOS of the tip has the Lorentz shape and centers at its Fermi energy $_T$ with width $_t$.

C. The free Green functions for magnetic atom

The main term produced the Kondo effect is the spin-flipping term, that is the last term in the Hamilton H_0. We assume the Hamilton had been solved exactly. The free Green function of magnetic atom including the Kondo resonance is calculated using the Hartree-Fock approximation with U^2 and U^4 order self energy.[47] The retarded Green function of the Anderson impurity is written as $G_d^r(!) = \frac{1}{! \ "^d + i}$ where $"^d = "^d + n \ U$. From the results of particle-hole symmetric Anderson model in reference,[46, 47] up to the U^2 and U^4 self energy, the $G_K(!)$ near zero frequency is written as

$$G_K(!) = \frac{1}{! \quad _2(!) + i} \tag{7}$$

$$_2(!) = \quad _R ! \quad i_I((\frac{!}{\quad})^2 + (\frac{T}{\quad})^2):$$

where $_R = (3 \quad \frac{^2}{4})(\frac{U}{\quad})^2 + 0.0553(\frac{U}{\quad})^4$, $_I = \frac{1}{2}(\frac{U}{\quad})^2 + 6(5 \quad \frac{}{2})(\frac{U}{\quad})^4$ and $= \quad _0 A^2$. We find from our calculations that it is enough up to U^2 term.

At zero temperature, the height of the peak is exactly $_0 = \frac{1}{}$. $_2(!)$ satisfies the general Fermi-Liquid properties $\mathrm{Im} \ _2(0) = 0$ and $\frac{d\mathrm{Im} \ _2(0)}{d!} = 0$ at zero temperature.[49] It is also a good approximation to asymmetric Anderson model in Kondo regime if the asymmetric Anderson model is still described approximately by Fermi liquid. The approximation has been used to study Kondo resonance on surface.[2] The main temperature effect is introduced by Eq. (7) and other temperature effects are introduced by Fermi distribution function $n_f(!)$.

The Green function of magnetic atom, similar to the reference,[20] is written as

$$g_d^r(!) = \hat{g}_d^r(!) + Z \ G_K(! \quad E); \tag{8}$$

where $G_K(!)$ is Kondo resonance peak and E is the shift of Kondo peak away from the Fermi energy. E is generally very small about several meV. The choice of Z, $(Z_"; Z_\#) = (1.0, 0.0)$, meets the condition that the height of Kondo peak is equal to $\frac{1}{}$ in the total density of state of magnetic atom. Instead of in reference [20] where the Kondo resonance is Lorentz shape, in this work the treatment of Kondo resonance is improved with non-Lorentz shape. The Green function $\hat{g}^r = \frac{1}{! \ "^d + i \ _d}$, where $_d$ doesn't include the contribution from the hybridizations with surface state and tip and doesn't contribute to Kondo resonance. $_d$ can be seen as the contributions from the bulk electrons [20, 50] or other complex interactions between the absorbed magnetic atoms and the surface, and treated as an input parameter. The scheme Eq. (7) isn't simple decoupling because the width and height of the decoupling Kondo resonance are dependent on the energy-level width and splitting of magnetic atom. The Friedel sum-rule Eq. (9) also tights the Kondo resonance and other parts of Green function together in the following self-consistent calculations. At present, the scheme only used in the study of Anderson model in Kondo regime.

TABLE I: The parameters for numerical calculations (unit eV). The band width for surface state is 4.0 eV

A	V	B	U	$"_d$	$_d$	$_t$
0.20	0.10	0.05	2.80	-0.80	0.30	1.00

D. Summary of self-consistent calculations

Up to now, we have known the free retard Green functions for the tip, surface and magnetic atom. Based on Eq. (A5), we can transform the retard Greens to the Matrix Green functions as the free matrix Green functions for non-equilibrium self-consistent loops. In this work, the trial Green functions $G_0^c(!)$ for the self-consistent calculations are equal to their free Green functions $G_0^c(!) = g^c(!)$. In the self-consistent loop we calculate the occupation number

$$n = \frac{1}{} \int_{1}^{Z_{+1}} d! f(! \quad _S) \mathrm{Im} G_d^r(!): \tag{9}$$

the new position of energy-level of magnetic atom $"^d = "^d + n \ U$ and the energy-level width $= \mathrm{Im} \ ^d(! = _S)$ which is the sum contributed from the hybridizations with surface state and tip. Thus the shape of Kondo resonance is also changed in each loop. If the changes of occupation numbers are smaller than 0.001, the occupation numbers, Green functions and self-energies converge simultaneously. The Friedel sum-rule Eq. (9) is satisfied and the self-consistent calculations stop.

The spectral functions are obtained by formula $A(!) = \frac{1}{2}(G^<(!) \quad G^>(!))$ and the density of State $(!) = \frac{1}{}A(!)$. The tunneling current is calculated using Eq. (4). The differential conductance is numerically calculated from the curve of the tunneling current via bias voltage. In our self-consistent perturbed calculations the basic equation $G + G^~ = G^> + G^<$ for the matrix Green function is only approximately satisfied with accuracy about from 0.001/eV to 0.01/eV.

IV. RESULTS AND DISCUSSIONS

In this work we concentrate on the small bias voltage. It is convenient to drop the indexes of $V_{n \ 0}, B_{nk \ 0}$

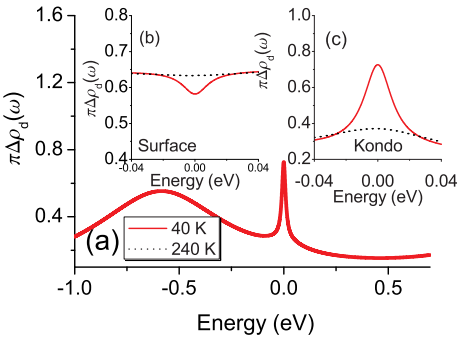

FIG. 3: The density of state for magnetic atom (a,c) and the surface (b) with A = 0.20 eV and U = 2.8 eV. The broad peak in (a) is the wide energy level for magnetic atom; the small sharp peak is the Kondo resonance. The solid line is the density of state (DOS) at 40 K and dot line at 240 K. The surface density of states and the detail structure of Kondo resonance are shown in the insert figure.

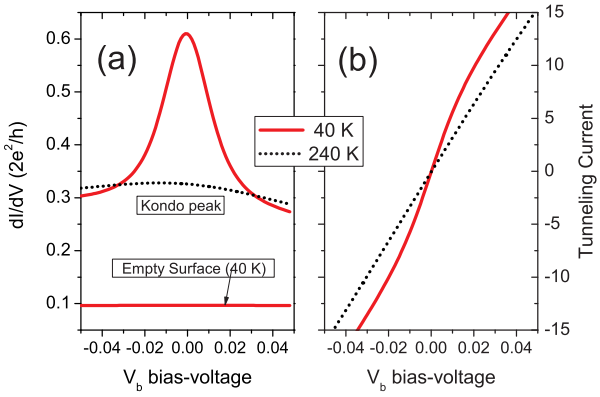

FIG. 4: (a). The tunneling spectra of magnetic atom constant energy-window [-2.0 eV, 2.0 eV] at near zero-bias voltage at temperatures 40K and 240 K. Kondo peak becomes flat at 240K above Kondo temperature about 100 K. The tunneling spectrum of empty surface at 40 K also plots in this figure. (b) The tunneling current at 40 K and 240 K when the tip on top of the magnetic atom.

and $A_k \to 0$ and simplify to V, B and A without introducing confusion. The model parameters are collected in table (I). The parameters are close to Kondo regime ($U < \varepsilon_d$) and close to the values for Co atom on Au(111) surface provided in reference.[20]. In Kondo regime, there is sharp Kondo resonance peak at Fermi energy besides the bare virtual resonance peak in the density of state of the absorbed magnetic atom.

A. Calculations of Density of state (DOS) and Differential conductance

The density of state of the absorbed magnetic atom and surface are shown in Fig. 3. From this figure [Fig. 3 (a)], we can find one broad peak of energy level of the magnetic atom. The sharp peak at Fermi energy of the surface is well known Kondo resonance. The Fig. 3(c) shows the effects of Kondo resonance, when temperature increasing above the Kondo temperature T_K. We estimate the Kondo temperature based on the width of Kondo Peak at zero temperature and find $T_K = 100$ K. The Kondo temperature T_K also is estimated based on the equation $D\sqrt{J}e^{-\frac{1}{J}}$ [43, 44], where is the density of state of surface at Fermi energy, $J = =(\ )[1=j\varepsilon_d j + 1=j\varepsilon_d + U j]$ obtained by Schrieffer-Wolf transformation [45] and D is the effective bandwidth of surface state contributed to Kondo effects. We estimate the Kondo temperature $T_K = 123$ K if 2D = 4 eV. The 2D is approximate to the energy windows in our calculations from -2 eV to 2 eV. The Fig. 3 (b) shows the density of state of the surface which is almost flat only there is a valley at the Fermi energy. The depression of surface DOS near Fermi energy is because some surface electrons at Fermi energy bind with the Anderson impurities and screen its local spin by forming spin-singlet binding state.

The peak structures of Kondo resonance have been found in the tunneling spectra of cobalt atom embedded in larger molecules absorbed on metal surfaces. [7, 8]. We calculate the differential conductance using the parameters in table (I) at temperature 40 K. The energy-range in the integral is from -2.0 eV to 2.0 eV, approximately from 1 to +1 in our calculations. We also calculate the tunneling spectrum of empty surface. From Fig. 4 (a) we can see that a peak appears at zero bias and it became flat at 240 K. It's just Knodo resonance in tunneling spectrum. If the tip move away from the magnetic atom to empty parts of the surface, the tunneling spectrum is flat. The peak structure of Kondo resonance and the flat spectrum for empty surface are celebrated because dI/dV curve is correspondent to the density of state and close to the prediction of the standard Terso 'S STM theory [13, 14].

B. Influence of energy-window and energy cutoff on shape of resonance peak

The dip structures are more common in STM tunneling spectrum. The energy-window of tunneling electrons has important influence on the shapes of dI/dV curves. Several theoretical works [18, 21] have shown that, in order to obtain correct tunneling spectra, the calculations of tunneling matrix need to use an energy-cutoff above Fermi energy to remove high-energy surface electrons. This is implicit that only part of electrons with proper energy-range can tunnel into the tip. At zero

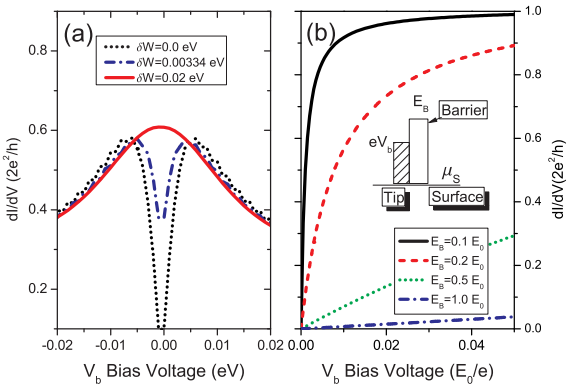

FIG. 5: (a) The energy-window influences the shape of dI/dV curve near zero-bias. Three different energy-windows are used $[-(eV_b + \quad E), (eV_b + \quad E)]$ $E = 0.0, 0.0034, 0.02$ (eV). (b) The dI/dV curves for single electron transmits through a square barrier with height E_B. The sharp dip structures are shown for small barriers. The insert figure illustrates the simplified STM device without absorbed atoms on surface. $E_0 = \frac{\hbar^2}{2ma^2}$ is a characteristic energy for the barrier

temperature, there exists clear energy-window with the Fermi energies of the tip and surface as its up-boundary and down-boundary. Only electrons with energies in the window can transmit to the other side of the barrier between the tip and surface and tunnel into the tip. The tip can't capture high-energy electrons although they have already transmitted the barrier.

At finite temperature, the energy distribution of electron becomes smoothly across the Fermi energy. We may add a skip-energy W to define energy-window at finite temperature to include more electrons and cutoff electrons with higher energy. We alter the energy-window to $[-(eV_b + \quad W), (eV_b + \quad W)]$ and calculate the dI/dV curve again. The width of energy-window changes with the bias voltage. In fact cutoff effect of Fermi energy has already included in our current formula by lesser Green functions and self energies for non-interaction case. After self-consistent calculations the electronic interactions of different parts are introduced. The cutoff effect of lesser Green functions becomes weak even at very low temperature and Fermi distribution still allows high-energy electrons above Fermi energy. We use the energy cutoff $eV_b + \quad W$ to neglect electrons with higher energies. The integral limits are symmetric around Fermi energy. From Fig. 5 (a), we can see that the dip structures appear when $W < 0.02$ (eV). For $W = k_B T = 0.00334$ (eV) < 0.02 (eV), there is a sharp dip structure. We can also find from Fig. 5 (a) that energy-window effect is only effective near zero bias. If the minimum value of effective energy-window is larger than 0.02 (eV), the influence of energy-window can be ignored.

Both the energy-window and energy-cutoff effects together determine the local minimum of dI/dV curve at zero bias. We must analyze them more deeply. At large bias voltage V_b the energies of most tunneling electrons are in energy-range from 0 eV to eV_b. The number of electrons with high-energies is relative small. At very small bias voltage, the number of electrons within the energy-range is deceased to very small value. At this time, if we remove high-energy electrons the total difference conductance will has a large decrease. Only W less than 0.02 eV, in another word, more high-energy electrons are removed the local minimum near zero-bias is more prominent.

We study a simplified STM model, that is, electrons transmits though a single barrier which is vacuum region between the tip and surface. From the insert figure of Fig. 5 (b), the height of the barrier is E_B and the energy of incident electron is E. By standard quantum mechanic calculation, the transmitting coefficient is

$$T(E) = \frac{1}{1 + \frac{E_B^2}{E(E_B - E)} \sinh^2\left(\frac{2ma^2}{\hbar^2}(E_B - E)\right)}; \qquad (10)$$

for $E < E_B$ where a is the width of the square barrier. The differential conductance is calculated by the Landauer-Buttiker type formula $G = \frac{2e^2}{h} T(eV_b)$. From the Fig. 5 (b). We find the sharp dip structure for small barrier. The transmission coefficients increase with energies of tunneling electrons. Compared with high-energy electrons, near zero bias the energies of tunneling electrons are small and the transmission coefficients are also small.

The dI/dV curves obtained from our model have similar shapes to the dI/dV curves for the single barrier model is indicative that the dip structures are because the energies of tunneling near low bias locate in classic forbidden regime of the vacuum barrier between the tip and surface. We remove the high-energy electrons by introducing energy-cutoff is equivalent that we restrict the energies of tunneling electrons below the effective barrier and within classic forbidden regime near zero bias. The number of high-energy electrons is small, but their transmission coefficient is large. They will have important influence on differential conductance because if at low bias most of electrons have low energies and small transmission coefficient. Although STM device has simple structure, many things are unclear such as the shape and size of tip. Generally the tip can't capture all tunneling electrons. At low bias, most of electrons locate in low-energy regime. The high-energy electrons and low-energy electrons are in different energy-scale so high-energy events are irrelevant to low-energy events. This is the reason why we introduce energy-cutoff to remove high-energy electron. The realistic STM devices are more complex. We must known the exact information of surface state. Of course, the directions of velocity of tunneling electrons also determine whether the tip can capture these tunneling electrons. Thus we suggest that, to more close to realistic STM, we should add a captured probability fac-

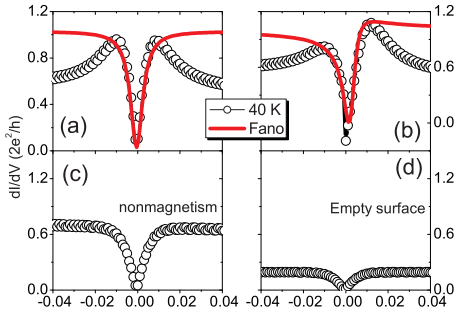

FIG. 6: The differential Conductance vs bias Voltage at 40 K with A = 0.20 eV, U = 2.8 eV. The solid lines with circles illustrate the results at 40 K. The Kondo temperatures T_K are about 100 K. The solid lines indicate the Fano shapes fitting the dI/dV curves at 40 K. The figure (b) is the asymmetric resonance when the Kondo peak shifts away the Fermi energy about 0.005 eV. (c) the dI/dV curve for nonmagnetic impurity and (d) for empty surface.

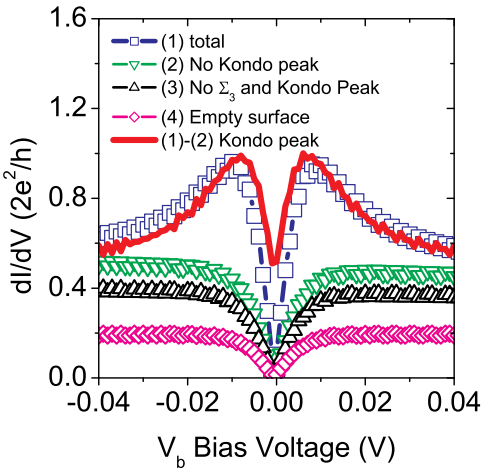

FIG. 7: (1) Open squares show the dI/dV curve for the full calculation including Kondo peak and (2) solid line with open down-triangles show the dI/dV curve without Kondo resonance (Eq. (7)) in self-consistent calculations. The (3) up-triangles for without both Σ_3 self-energies and Kondo peak, and the (4) diamonds for empty surface are also plotted in this figure. The contribution of Kondo resonance to dI/dV curve (bold thick-solid line) is obtained by having subtracted (2) from (1).

tor $W(\omega)$ into the current formula, and it can be written as $J = \frac{2e}{h}\int W(\omega)T(\omega)d\omega$, where $T(\omega)$ is transmission coefficient. In this paper, $W(\omega) = \Theta(\omega - \mu) - \Theta(\omega + eV_b - \mu)$. This is just equivalent to the introduction of energy-window in our calculations. This is also equivalent to limit all tunneling matrixes with non-zero values only in this energy-window just like in reference. [18, 21] Besides energy, $W(\vec{r}\vec{r}\vec{r})$ could include position, momentum and any other more complex properties of STM device.

Based on our results, the dip structures in dI/dV curve near zero-bias are induced by the tunneling among the tip, absorbed atom and surface because the energies of tunneling electrons are smaller than heights of effective barriers of corresponding tunneling process. Not only most of many-body events but also subsequent single tunneling events are suppressed. The electronic tunneling events include subsequent single tunneling, co-tunneling and more complex tunneling process. If the background noises are reduced by proper method, the dip structure can be found in the dI/dV curve. If there are magnetic atoms on surface, Kondo resonance will enhance the differential conductance near zero bias, the dip structure has chance to be observed by modulating the shape of Kondo resonance. Thus the most of Kondo resonance observed in STM tunneling spectra are modulated by a local minimum.

C. Calculations of differential conductance with proper energy-cutoff

In this section we will study STM tunneling spectrum for the same parameters as in section A but we use a energy-cutoff from 0 eV to eV_b (see Fig. 1). The Eq. (B 8) is well common used formula for the calculations of electronic transport near zero temperature. The results are consistent with most of STM tunneling spectrum of magnetic atoms on metal surface. The differential conductance (dI/dV) is plotted in Fig.6(a). After having fitted the dI/dV curves at 40 K with Fano shape $\frac{(q+\varepsilon)^2}{1+\varepsilon^2}$ where $\varepsilon = \frac{\omega - \omega_q}{k_B T_q}$, we get Fano parameter q= 0.0 for (a) which is good fitting with Fano line-shapes. The symmetric resonant peak has been found in the STM tunneling spectra of Co/Au(111) and Co/Ag(111) [4]. Experimentally, some STM tunneling spectra of magnetic atoms on fcc(111) surface of novel metals are asymmetric dips [1, 3] or peaks.[2]. We shift the position of Kondo resonance about E = 0.005 eV away from the Fermi energy. We obtain asymmetric resonance peak very close the shape observed in experiments [1, 3] and q values by fitted with the Fano-line-shape is 0.30 for Fig.6(b).

In the nonmagnetic calculation the parameters are the same but U = 0. The clear dip structure is found from the dI/dV curve (Fig.6(c)). For the empty surface without absorbed magnetic atoms the dI/dV curve has also a dip structure near zero-bias. There is no dip structure in the density of the state of the nonmagnetic impurity and empty surface at the Fermi energies. Thus dip in dI/dV curve is the tunneling phenomenon such as single tunneling and co-tunneling events. The magnetic impurity and even nonmagnetic can enhance the dip structure. The resonant structures near zero bias for nonmagnetic impurities are found in other non-equilibrium calculation such as in reference. [22]

D. The detail analysis of dI/dV curves

We analyze the dI/dV curves in detail. In the current formulation Eq. (4), the tunneling current is the sum of two parts J_1 and J_2. J_1 is proportional to the image part of the retarded Green function of the tip (or the density of state of the tip $_{ct}(!) = \frac{1}{}\mathrm{Im}\,G^{ct(r)}(!)$) and represents the tunneling from the surface and absorbed atom into the tip. J_2 is proportional to the density of electrons ($G^{<}_{ct}$ / n) at the tip which represents the tunneling from the tip to the surface and absorbed atom. Experimentally, the shape of Kondo resonance in dI/dV curve, which is the mixing of Kondo resonance and others zero-bias structures, is not exactly the shape of Kondo resonance in the spectral function or density of state just like we have already discussed in the section B. The kondo resonance generally is modulated by a dip structure near zero-bias.

We omit the Kondo Peak term Eq. (7) in the free Green function of the magnetic atom Eq. (8) and calculate the dI/dV curve again. We can find that from Fig. 7, the dI/dV curve is a dip. There is also a dip for empty surface when we remove the magnetic atom away from the surface. The dip generally becomes flat as increasing temperature. The behavior is similar to another important zero-bias phenomenon besides the Kondo resonance, the so-called zero-bias anomaly.[51] If we subtract the dip from total dI/dV curve we get the Kondo resonance Peak (solid-line).

The orthogonality catastrophe [29] of surface electrons prevents some many-body electronic transmission process. From the dI/dV curve we can find a local minimum near zero-bias, this is so-called zero-bias anomaly. The cotunneling mechanism has also contributions to the zero-bias anomaly even for nonmagnetic atom or quantum dot.[30, 31] In this work the anomaly dip doesn't come from the orthogonality catastrophe because there aren't directly electronic interactions for the surface and tip. However the orthogonality catastrophe will contribute part of height of tunneling barrier from the surface to tip. The co-tunneling has been included in our model and self-consistent calculations. From Fig. 1 and the Feynman diagram in Fig. 2 for the Dyson equations, we can see that physics of co-tunneling is mainly included in the $_3$ self-energies for the tip, surface and magnetic atom, such as an electron jumps to spin-up state under the Fermi energy after a spin-up electron having already jumped to the surface. In order to prominently illustrate the effects of co-tunneling, we drop the $_3$ self-energies from the Dyson equations and calculate the dI/dV curve again. We find from Fig. 7 that the differential conductance decreases slightly. Remain dip structure is induced by subsequent single tunneling and higher power co-tunneling process embodied in the iterated calculations of the Dyson equations. The co-tunneling events do happen with short time interval and they only play the role of virtually intermediate states in perturbed calculations, but still have important influence on real physical tunneling.

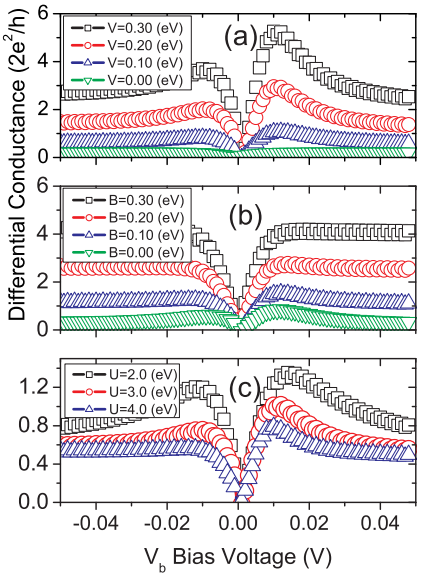

FIG. 8: The dI/dV curves change with (a) the amplitudes V from magnetic atom to tip, (b) B from surface to tip and (c) on-site Coulomb energy U at 40 K

In the absence of the Kondo resonance, no dip structure near Fermi energies in the densities of state of the tip, magnetic atom and the surface show that the dip in dI/dV curve is dynamically tunneling phenomenon. Our results also indicate that the contributions of co-tunneling to zero-bias anomaly are not too large, but others tunneling events such as the subsequent single tunneling and the higher order co-tunneling contribute most parts of zero-bias anomaly. When Kondo resonance happens in the present of magnetic impurity, there is a dip structure in the density of state of surface conducting electron [Fig.3 (b)]. This contributes an additional dip structure to dI/dV curve, which mixes with the dip structure coming from dynamically tunneling. The dip structures have the widths with the same energy scale as the system temperature. If the Kondo temperature is higher than system temperature, the Kondo resonance is still modulated by the remain weaker dip structure [see Fig.7] and the Kondo resonance at first sight splits two peaks. The total shape of dI/dV curve is the mixing of two splitting peaks and main strong dip structure.

E. Influence of tunneling amplitudes and electronic correlations

The change of the tunneling current of STM is very significant when we change the distance from the tip to surface. The tunneling matrix V or B represents the tunneling from the absorbed atom or the surface to the tip.

V and B are proportional to $e^{d(r)/\lambda}$, where d(r) is the distance from the tip to point r on the surface. The smaller is d the larger is V or B. Thus, when the tip continuously accesses the surface or adsorbed atom, the parameter V or B changes from smaller value to larger one. Fig. 8(a) illustrates the resonance peaks in dI/dV curves become stronger and asymmetric when V increases from small to large values. In calculations, we shift the Kondo resonance about E = 0.005 eV above Fermi energy. We can also see that the Kondo resonance appears more prominent at strong tunneling in dI/dV curves. From Fig. 8(b) we also see that strong tunneling from surface to tip makes the shape of dI/dV curves are more symmetric. This is because, at strong tunneling from the surface to tip, the role of the absorbed magnetic atom becomes less important. The electron-correlation interaction plays an important role for Kondo effect. Based on the Yosida and Yamada's calculations [46, 47], for strong coulomb interaction (large U) the Kondo resonance sharp but weak with small area closed by the energy-axis. After having calculated the dI/dV curves, we find the Kondo resonance more peak alike but weak as having increased U from 2.0 eV to 4.0 eV.

V. SUMMARY AND CONCLUSION

The STM tunneling spectra are obtained using the non-equilibrium self-consistent calculations. The dI/dV curves have Fano's shapes and are close to the experimental tunneling spectra of 3d transition-metal atoms on novel-metal surface. The Kondo resonance in measurements dI/dV curves generally are the mixture of pure Kondo resonance and the dip structure due to others zero-bias anomaly such as the subsequent single tunneling, cotunneling and other more complex tunneling events in the STM device. If Kondo resonance is strong the dI/dV curve is peak near zero-bias voltage and its shape is modulated by a valley or dip. Based on our model, the energy-window of tunneling electron has significant influence on the tunneling spectrum at very near zero-bias. The energy-window effect is unimportant for large bias voltage.

On the one hand, Anderson model can't capture all information in detail on the STM device, but it still captures the most important properties of STM device. Our calculations only provide the main characters of Kondo resonance in STM device. More accurate calculations need to find a model more close to the real STM experiments and know the exact information on surface state.

In this paper we have also developed a computational method of non-equilibrium electronic transport which is not only fit for STM device but also quantum dot, nanomolecule-device, hybridization system of normal metal and superconductor and others mesoscopic transport system. The self-consistent method can be extended to the system far beyond equilibrium by replace single-time integral and single-frequency Fourier transformation with double-times integral and double-frequency Fourier transformation. The method is suitable to the real time and real-space to study the pattern of tunneling spectrum on a surface.

Acknowledgements

The author are greatly indebted to Prof. Z. Zeng, Dr J. L. Wang and X. Q. Shi for their helpful suggestions and Dr. X. H. Zheng for having carefully read the first version of the manuscript. This work is financially supported by Nature Science Foundation of China and Knowledge Innovation Program of Chinese Academy of Sciences under KJCX2-SW-W11. This work had been partially running on the computers located at Center for computational science, Hefei Institutes of Physical Science, Chinese Academy of sciences.

APPENDIX A: NON-EQUILIBRIUM GREEN FUNCTION AND SCHWINGER-KELDYSH CONTOUR

Schwinger and Keldysh [32, 33] introduced a time contour or closed time path shown in the schematic diagram below which includes a positive branch c_+ from -1 to $+1$ and a negative branch c_- from $+1$ to -1.

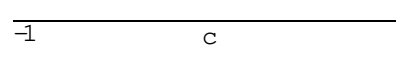

A new Green function is introduced on the contour, which is expressed as $G^c(t,t') = -i\langle T_c A(t)^\gamma B(t')\rangle$, T_c is an operator ordering the operators along the contour. If both t and t' are on the positive branch of the contour, T_c is equivalent to the usual time-ordering operator and the Green function is the usual time Green function $G(t,t') = -i\langle TA(t)^\gamma B(t')\rangle$. If both t and t' are on the negative branch of the contour, T_c is expressed as $\tilde{T}$ which orders operators from $+1$ to -1. The Green function expresses as $G^{\sim}(t,t') = -i\langle \tilde{T}A(t)^\gamma B(t')\rangle$. If t is on the positive branch and t' is on the negative branch, the order of operators is well organized and T_c is omitted, the Green function $G^<(t,t') = i\langle A(t')^\gamma B(t)\rangle$ is the lesser Green function. If t is on the negative branch and t' is on the positive branch, the order of operator is converted and T_c is omitted, the Green function is the greater Green function and is written as $G^>(t,t') = -i\langle A(t)B(t')^\gamma\rangle$.

By introducing the time contour, Feynman rules, Wick theorem and the Dyson equation are the same as that at zero temperature. The only difference is that the time integration now is along the contour and the time can be at different branches of the contour. The Dyson equation can be projected on the positive branch $(-1, +1)$. If considering t and t' probably at different branches of

the contour, there are four Dyson equations which can regroup into a matrix equation [34]

$$G^c = \begin{matrix} G & G^< \\ G^> & G^\sim \end{matrix}; \quad {}^c = \begin{matrix} & {}^< \\ {}^> & {}^\sim \end{matrix}; \quad g^c = \begin{matrix} g & g^< \\ g^> & g^\sim \end{matrix}: \tag{A1}$$

$$G^c(t;t^0) = g^c(t;t^0) + \int_{c^+} dt_1 \int_{c^+} dt_2 g^c(t;t_1)\ {}^c(t_1;t_2)G^2(t_2;t^0): \tag{A2}$$

Now the contour Green function can be calculated in the same manner as that at zero temperature. The only difference is that complex Green functions and self energies are replaced by the complex matrixes of Green functions and self energies. In this work, we mainly study the electronic transport at small bias. We assume the STM work in the non-equilibrium stationary state. [35] On the other hand the matrix Green functions define on only the positive branch. Thus, there is still the time translation invariance after the system enters into the non-equilibrium stationary state. The matrix Green functions are dependent on the relative time interval $G^c(t\ t^0)$. In energy space, the Dyson equation is more simple under the non-equilibrium stationary state and written as

$$G^c(!) = g^c(!) + g^c(!)\ {}^c(!)G^c(!): \tag{A3}$$

The retarded and advanced Green functions are calculated using

$$\begin{aligned} {}^r(!) &= \quad (!) \quad {}^<(!); \quad {}^a(!) = \quad (!) \quad {}^>(!) \\ G^r(!) &= G\ (!) \quad G^<(!) = G^>(!) \quad G^{\sim(!)} \\ G^a(!) &= G\ (!) \quad G^>(!) = G^<(!) \quad G^\sim(!): \end{aligned} \tag{A4}$$

In our calculations we have used following important properties of the matrix Green functions which can be derived from the symmetry of non-equilibrium Green function $G^{<(>)}(!) = \quad G^{<(>)}(!)$, $G\ (!) = \quad G^\sim(!)$, $G^r(!) = G^a(!)$ and the Kubo-Martin-Schwinger condition $G^<(!) = \quad e^{(!\ )}G^>(!)$ [35]

$$\begin{aligned} G^<(!) &= \quad 2in_F(!)\mathrm{Im}G^r(!); \\ G^>(!) &= \quad 2i(n_F(!)\quad 1)\mathrm{Im}G^r(!) \\ G\ (!) &= \mathrm{Re}G^r(!)\quad i(2n_F(!)\quad 1)\mathrm{Im}G^r(!); \\ G^\sim(!) &= \quad \mathrm{Re}G^r(!)\quad i(2n_F(!)\quad 1)\mathrm{Im}G^r(!): \end{aligned} \tag{A5}$$

. where $n_f(!)$ is the Fermi distribution function.

APPENDIX B: DERIVATION OF THE TUNNELING CURRENT FORMULATION

It is convenient to calculate the contour Green function directly, not the lesser Green function. The mixing Green function in the current formulism (Eq.3) can be defined on the contour and the full mixing contour Green function can be expressed using the Green functions of the tip, the adsorbed atom and the surface based on the methods in the reference.[40]

$$\begin{aligned} ht^y_n\ (t^0)d_{\ 0}(t)i_c &= \frac{1}{\sim}\sum_{n^0ss^0}\int_c dt_0 G_{nn^0s^0}\ (t_0;t^0)V_{n^0ss^0}g^{cd}_{s\ 0}(t_0;t) \\ ht^y_n\ (t^0)p_{k\ 0}(t)i_c &= \frac{1}{\sim}\sum_{n^0k^0ss^0}\int_c dt_0 G_{nn^0s^0}\ (t_0;t^0)B_{n^0k^0ss^0}g^{cp}_{kk^0s\ 0}(t_0;t); \end{aligned} \tag{B1}$$

s and s^0 are spin index. From the reference,[40] if $A(t;t^0) = \int_c dt_1 B(t;t_1)C(t_1;t^0)$ then

$$A^<(t;t^0) = \int_{c^+} dt_1 B^r(t;t_1)C^<(t_1;t^0) + B^<(t;t_1)C^a(t_1;t^0) \tag{B2}$$

After the contour Green function having projected onto the positive branch, the lesser Green function having inserted into the current formulation and the current formulation having been reorganized, the current is writ-

ten as $\langle J_T \rangle = J_1 + J_2$, where

$$J_1 = \frac{2e}{\sim^2} Re[\sum_{nn's} \int_{c^+} dt_0 G^{ct(r)}_{nn's}(t_0, t) T^{ct(<)}_{nn's}(t_0, t)] \quad (B3)$$
$$= \frac{2e}{h} Re[\sum_{nn's} \int d! [G^{ct(r)}_{nn's}(!) T^{ct(<)}_{nn's}(!)]$$
$$= \frac{2e}{h} \int d! ReTr[G^{ct(r)}(!) T^{ct(<)}(!)]$$
$$J_2 = \frac{2e}{\sim^2} Re[\sum_{nn's} \int_{c^+} dt_0 G^{ct(<)}_{nn's}(t_0, t) T^{ct(a)}_{nn's}(t_0, t)]$$
$$= \frac{2e}{h} Re[\sum_{nn's} \int d! G^{ct(<)}_{nn's}(!) T^{ct(a)}_{nn's}(!)]$$
$$= \frac{2e}{h} \int d! ReTr[G^{ct(<)}(!) T^{ct(a)}(!)]:$$

and the first equation converts to the second equation by using the Fourier transformations under the same assumption of non-equilibrium stationary state as the Dyson equations Eq.(A3). The T matrixes are written as,

$$T^{ct(<)}_{nn's}(!) = \sum_{kk's'0'0} B_{nk0'0} B_{n'0k's's0} g^{cp(<)}_{kk's'0'0}(!) \quad (B4)$$
$$+ \sum_{s'0'0} V_{n0'0} V_{n's's0} g^{cd(<)}_{s'0'0}(!)$$
$$T^{ct(a)}_{nn's}(!) = \sum_{kk's'0'0} B_{nk0'0} B_{n'0k's's0} g^{cp(a)}_{kk's'0'0}(!)$$
$$+ \sum_{s'0'0} V_{n0'0} V_{n's's0} g^{cd(a)}_{s'0'0}(!):$$

$g^{cp(<)}_{kk's'0'0}$ and $g^{cd(<)}_{s'0'0}$ are the free Green functions of the absorbed atom and the surface. In order to calculate contour Green function, at first, the self-energy is calculated. Based on Feynman diagrams [Fig.2], the self energies of the absorbed atom and the surface can be calculated using the following formulations:

$$^{cd}(!) = \sum_{n'0'0n''0''0''0''} V_{n'0'0} V_{n''0''0''} g^{ct}_{n'0'n''0''0''0''}(!) \quad (B5)$$
$$+ \sum_{k'0'k''0''0''} A_{k'0'0} A_{k''0''0''} g^{cp}_{k'0'k''0''0''0''}(!) + ^{cd}_{3}(!)$$
$$^{cp}_{kl}(!) = \sum_{n'0'0kn''0''0''} B_{n'0'0k} B_{n''0''0l} g^{ct}_{n'0'n''0''0''0''}(!)$$
$$+ \sum_{0'0''} A_{k0'} A_{l0''} g^{cd}_{0'0''}(!) + ^{cp}_{3kl}(!)$$
$$^{ct}_{mn}(!) = \sum_{0'0} V_{m0'} V_{n0'} G^{cd}_{0'0}(!)$$
$$+ \sum_{k'0'l'0'0'} B_{mk'0'} B_{nl'0'} G^{cp}_{k'0'l'0'0'}(!) + ^{ct}_{3mn}(!);$$

and are the spin index. The $_3$ self energies for the tip, adatom and surface are expressed as

$$^{cp}_{3kl}(!) = \sum_{mn'0'0''0''} B_{mk'0} V_{n'0'0''} A_{l''0''} g^{cd}_{0''0''}(!) g^{ct}_{mn'0'0'}(!) \quad (B6)$$
$$+ \sum_{mn'0'0''0''} A_{k'0} V_{m'0'0''} B_{ml''0''} g^{ct}_{mn'0''0''}(!) g^{cd}_{0'0'}(!)$$
$$^{ct}_{3mn}(!) = \sum_{k'l'0'0'0''0''} V_{m'0} A_{k'0'0''} B_{nl'0''} g^{cd}_{0'0'}(!) g^{cp}_{k'0'l'0''0''}(!)$$
$$+ \sum_{k'l'0'0'0''0''} B_{mk'0} A_{l'0'0''} V_{n''0''} g^{cp}_{k'0'l'0'0'}(!) g^{cd}_{0''0''}(!)$$
$$^{cd}_{3}(!) = \sum_{mnk'l'0'0'0''0''} A_{k'0} B_{ml'0'0''} V_{n''0''} g^{cp}_{k'0'l'0'0'}(!) g^{ct}_{mn'0''0''}(!)$$
$$+ \sum_{k'l'0'0'0''0''} V_{m'0} B_{nk'0'0''} A_{l'0''} g^{ct}_{mn'0'0'}(!) g^{cp}_{k'0'l'0''0''}(!):$$

which presents the cotunneling events in the STM device. A typical cotunneling event is that an electron jumps to the surface and leaved a hole on the magnetic atom, and subsequently a tip electron fills the hole on the magnetic atom [Fig. 1 and Fig. 2]. For higher-order cotunneling processes include more electrons and tunneling events which generally are included in the iterated calculations. By compared the matrix expression of self-energy with the matrix expression of T matrix in the current formulation, T is just the lowest order approximation of the

exact self-energy. In our current formulation T replaces by the self-energy in Eq. (B3).

$$J_1 = \frac{2e}{h}\int_{-1}^{+1} d! \, ReTr[G^{ct(r)}(!) \; {}^{ct(<)}(!)] \quad (B7)$$

$$J_2 = \frac{2e}{h}\int_{-1}^{+1} d! \, ReTr[G^{ct(<)}(!) \; {}^{ct(a)}(!)]:$$

When near zero bias the electronic tunneling is in classic forbidden regime, we use following current formula with energy cutoff

$$hJ_T i = J_1 + J_2 \quad (B8)$$

$$J_1 = \frac{2e}{h}\int_{-1}^{+eV_b} d! \, ReTr[G^{ct(r)}(!) \; {}^{ct(<)}(!)]$$

$$J_2 = \frac{2e}{h}\int_{-1}^{+eV_b} d! \, ReTr[G^{ct(<)}(!) \; {}^{ct(a)}(!)]:$$

where if positive bias voltage applies to surface $V_b > 0$. is equal to $_S$ the chemical potential of the surface. Because of numerical reason $_S$ sets to zero value to keep the position of Kondo peak unchange. The bias-voltage is applied by changing the chemical potential of the tip in our numerical calculations. $_S$ keeps zero when applying a small bias voltage V_b on the surface mean that applying a bias voltage to the tip $V_t = -V_b$.

In real calculations, we add a minus ahead the current formulas Eq.(4), Eq.(B7) and Eq.(B8)) to make the current $J_T = J_1 + J_2 > 0$ at positive bias once the lower bound and up-bound of the integrates are clearly written in the current formulas. We can adopt the chemical potential langue just like in Ref [39] without introducing additional minus in the current formulas. The basic reason of the difference is that the increase of chemical potential of electron is equal to $-e\,V_b$

[1] V. Madhavan, W. Chen, T. Jamneada, M. F. Crommie, and N. S. Wingreen, Science 280, 567 (1998).
[2] K. Nagaoka, T. Jamneada, M. Grobis, and M. F. Crommie, Phys. Rev. Lett. 88, 077205 (2002).
[3] N. Knorr, M. A. Schneider, Lars Diekhoner, P. Wahl, and K. Kern, Phys. Rev. Lett. 88, 096804 (2002).
[4] M. A. Schneider, L. Vitali, N. Knorr, and K. Kern, Phys. Rev. B 65, R121406 (2002).
[5] T. Jamneala, V. Madhavan, W. Chen, and M. F. Crommie, Phys. Rev. B 61, 9990 (2000).
[6] Jiutao Li, Wolf-Dieter Schneider, Richard Berndt, Bernard Delley, Phys. Rev. Lett. 80, 2893 (1998).
[7] Aidi Zhao, Qunxiang Li, Lan Chen, Hongjun Xiang, Weihua Wang, Shuan Pan, Bing Wang, Xudong Xiao, Jinlong Yang, J. G. Hou, Qingshi Zhu, Science 309, 1542 (2005).
[8] P. Wahl, L. Diekhoner, G. Wittich, L. Vitali, M. A. Schneider, and Kern, Phys. Rev. Lett. 95, 166601 (2005).
[9] V. Madhavan, T. Jamneada, K. Nagaoka, W. Chen, Je-Luen Li, Steven G. Louie, and M. F. Crommie, Phys. Rev. B 66, 212411 (2002).
[10] Y. B. Kudasov, and V. M. Uzdin, Phys. Rev. Lett. 89, 276802 (2002).
[11] H. C. Manoharan, C. P. Lutz, and D. M. Eigler, Nature(London) 403, 512 (2000).
[12] G. A. Fiete, and E. J. Heller, Rev. Mod. Phys. 75, 933 (2003).
[13] J. Tersoff, and D. R. Hamann, Phys. Rev. Lett. 50, 1998 (1983).
[14] J. Tersoff, and D. R. Hamann, Phys. Rev. B 31, 805 (1985).
[15] J. Bardeen, Phys. Rev. Lett. 6, 57 (1961).
[16] C. Bracher, M. Riza, and M. Kleber Phys. Rev. B 56, 7704 (1997).
[17] A. Schiller, and S. Hershfield, Phys. Rev. B 61, 9036 (2000).
[18] Chiung-Yuan Lin, A. H. Castro Neto, and B. A. Jones, arXiv:cond-mat/0307185 (2003).
[19] H. G. Luo, T. Xiang, X. Q. Wang, Z. B. Su, and L. Yu, Phys. Rev. Lett. 92, 256602 (2004).
[20] O. Ujsaghy, J. Kroha, L. Szunyogh, and A. Zawadowski, Phys. Rev. Lett. 85, 2557 (2000).
[21] J. Merino, and O. Gunnarsson, Phys. Rev. B 69, 115404 (2004).
[22] M. Plihal, and J. W. Gadzuk, Phys. Rev. B 63, 085404 (2001).
[23] A. C. Hewson, The Kondo Problem to Heavy Fermions, Cambridge University Press (1993).
[24] Piers Coleman, Phys. Rev. B 29, 3035 (1983).
[25] N. E. Bickers, Reviews of Modern Physics, 59, 845 (1987).
[26] K. Schonhammer, Solid State Communications, 22, 51 (1977).
[27] H. Kajueter, and G. Kotliar, Phys. Rev. Lett. 77, 131 (1996).
[28] O. Gunnarsson, and K. Schonhammer, Phys. Rev. B 28, 4315 (1983).
[29] P. W. Anderson, Phys. Rev. Lett. 18, 1049 (1967).
[30] S. De Franceschi, S. Sasaki, J.M. Elzerman, W. G. van der Wiel, S. Tarucha, and L.P. Kouwenhoven, Phys. Rev. Lett. 86, 878 (2003).
[31] I. Weymann, J. Barnas, J. Konig, J. Martinek, and G. Schon, arXiv:cond-mat/0412434, (2004).
[32] J. Schwinger, J. Math. Phys. 2, 407 (1961).
[33] L. V. Keldysh, Zh. Eksp. Teor. Fiz 47, 1515 (1964); [Sov. Phys. JETP 20, 1018 (1965)]
[34] Gerald D. Mahan Many-Particle Physics (Second Edition) chapter 2, Plenum Press (1990);
[35] Guang-zhao Zhou (K. C. Chou), Z. B. Su, B. L. Hao, and L. Yu, Physics Reports 118, 1-131 (1985); J. Rammer and H. Smith, Reviews of Modern Physics, 58, 323 (1986).
[36] Alex Kamenev, Lecture Notes Presented at Windsor NATO School on "Field Theory of Strongly Correlated Fermions and Bosons in Low-Dimensional Disordered System" (August 2001). arXiv:cond-mat/0109316 (2001).
[37] C. Caroli, R. Combescot, P. Nozieres, and D. Saint-James, J. Phys. C: Solid St. Phys. 4, 916 (1971).
[38] Yigal Meir, and N. S. Wingreen, Phys. Rev. Lett. 68,

2512 (1992).
[39] N. S. Wingreen, and Yigal Meir, Phys. Rev. B 49, 11040 (1994).
[40] Antti-Pekka Jauho, N. S. Wingreen, and Yigal Meir, Phys. Rev. B 50, 5528 (1994).
[41] Baigeng Wang, Jian Wang, and Hong Guo, Phys. Rev. Lett. 82, 398 (1999).
[42] M. P. Anantram, and S. Datta, Phys. Rev. B 51, 7632 (1995).
[43] F. D. M. Haldane, Phys. Rev. Lett. 40, 416 (1978).
[44] K. G. Wilson, Rev. Mod. Phys. 47, 773 (1975).
[45] J. R. Schrieffer, and P. A. Wolff, Phys. Rev. 149, 491 (1966).
[46] K. Yosida and K. Yamada, Supplement of Progress of Theoretical Physics, 46, 244 (1970).
[47] K. Yamada, Progress of Theoretical Physics, 53, 970 (1975).
[48] H. Kaga, H. Kube, and T. Fujiwara, Phys. Rev. B 37, 341 (1988).
[49] J. M. Luttinger, Phys. Rev. 121, 942 (1960).
[50] Oded Agam, and Avraham Schiller, Phys. Rev. Lett. 86, 484 (2001).
[51] J. M. Rowell and L. Y. L. Shen, Phys. Rev. Lett. 17, 15 (1966).